applied sciences

MDPI

Article

The Impact of Vegetation Roots on Shallow Stability of Expansive Soil Slope under Rainfall Conditions

Yangming Wang *, Weisheng Xu, Zhe Wang and Yingna Zhu

Key Laboratory of Health Intelligent Perception and Ecological Restoration of River and Lake, Ministry of Education, Hubei University of Technology, Wuhan 430068, China
* Correspondence: 102100796@hbut.edu.cn; Tel.:+86-186-7048-4099

Abstract: The impact of reinforcing vegetation roots on the stability of expansive soil slopes with moisture absorption and expansion was investigated. Then, poinsettia is selected as the slope protection plant, and ABAQUS software (version 2022) with secondary development is used to simulate the moisture absorption and expansion of the expansive soil slope. After that, the strength reduction method is employed to study the effects on the displacement and plastic zone, and on the shallow layer of the expansive soil slope at different rainfall conditions. The following points are revealed: (1) The roots of the poinsettia can reduce the displacement of the slope. But, when the rainfall intensity exceeds the soil permeability coefficient, the soil reinforcement effect decreases. (2) The poinsettia root system can alleviate the concentration of plastic strain, disperse the plastic zone, and increase slope stability along the distribution of the roots. (3) The poinsettia roots can improve the shallow stability of the slope. But when the rainfall intensity exceeds the surface permeability coefficient, the magnitude of the reinforcement decreases. The results demonstrate that the poinsettia roots can enhance shallow slope stability. However, with increasing rainfall intensity, the ability of the poinsettia roots to enhance shallow slope stability gradually weakens.

Keywords: expansive soil; root reinforcement; rainfall; slope stability; slope displacement

check for updates

Citation: Wang, Y.; Xu, W.; Wang, Z.; Zhu, Y. The Impact of Vegetation Roots on Shallow Stability of Expansive Soil Slope under Rainfall Conditions. *Appl. Sci.* **2023**, *13*, 11619. https://doi.org/10.3390/app132111619

Academic Editor: Xilin Lv

Received: 14 September 2023
Revised: 19 October 2023
Accepted: 20 October 2023
Published: 24 October 2023

Copyright: © 2023 by the authors. Licensee MDPI, Basel, Switzerland. This article is an open access article distributed under the terms and conditions of the Creative Commons Attribution (CC BY) license (https://creativecommons.org/licenses/by/4.0/).

1. Introduction

Expansive soils are characterized by their main constituents, such as montmorillonite, illite, and other hydrophilic minerals, thus widely distributed and exhibiting the property of swelling upon wetting and cracking upon drying [1]. The unique properties of expansive soils can cause significant hazards, including slope instability. Currently, both domestical and international researchers have primarily focused on studying the moisture-induced swelling effect of expansive soils from a mechanical property perspective, investigating the decrease in shear strength caused by the swelling effect [2]. Xiao et al. [3] analyzed the relationship between saturation degree, temperature, and thermal expansion coefficient of expansive soils, simulated the swelling effect caused by moisture absorption, and identified it as a significant factor contributing to shallow layer slope failure in expansive soils. Zhao et al. [4] considered changes in matric suction, softening upon contact with water, and moisture-induced swelling. They simulated the influence of multiple wet-dry cycles under rainfall conditions on the stability of expansive soil slopes and found that slope failure mainly occurred in the shallow weathered zone, with moisture absorption-induced softening being the primary cause. Zhang et al. [5] considered the coupling effects in expansive soil slopes and established calculation formulas for overlying load taking into account the saturation degree, confirming that the initial water content of the surface layer is an important factor affecting slope stability. Xiao et al. [6] considered load-induced expansion and wet-dry cycles, combined with laboratory testing, and found that a low effective cohesion is a significant factor leading to surface layer failure in expansive soil slopes. He et al. [7] studied the influence of low stress and wet-dry cycles on the shear strength of expansive soil slopes and established a numerical model with nonlinear distribution of shear strength.

Vegetation slope stabilization relies on the combined action of the above-ground stems and leaves of plants and their underground root systems to reinforce, anchor, and support the soil, thereby achieving the goal of soil reinforcement and slope stability [8–10]. Currently, research on vegetation for slope stabilization mainly focuses on investigating the influence of plant root systems on the shear strength of soil from a mechanical perspective. Thomas et al. [11] conducted experiments and found that during landslide processes, the uphill-growing root systems tend to fracture and fail first, while the downhill-growing root systems experience compression before being subjected to shear forces. Reubens et al. [12] experimentally verified that when the angle between the root system and the shear plane is acute, it increases the shear strength of the soil, with the maximum reinforcing effect achieved at an angle of 60°. Conversely, when the angle is obtuse, it reduces the shear strength of the soil, with the minimum shear strength observed at an angle of 120°, which may even result in a negative reinforcing effect, where the shear strength of the soil is lower than that of unreinforced soil. The axial force generated by plant root systems in the shear zone of a slope depends on the angle between the roots and the shear plane, as well as the position of the roots relative to the shear plane. The shear strength of the slope soil also needs to consider the influence of root diameter and depth [13–15]. Kokutse et al. [16] conducted experiments to determine the relationship between root depth and additional cohesion, and used the strength reduction method to analyze the soil reinforcement effect of different vegetation root systems on common soils. Capobianco, Vittoria et al. [17], considering both the intrinsic cohesion of the soil and the additional cohesion generated by the roots, conducted numerical simulations to study the slope stability in the presence of grass, shrubs, and trees. Sui, ZiFan et al. [18] studied the impact of different rainfall intensities on the stability of slopes with various grass and shrub vegetation. Sun, Yang et al. [19] conducted laboratory hydraulic erosion tests to investigate the characteristics of runoff, sediment yield, and sheet flow velocity on tailings dam slopes under four different plant conditions: goosegrass, vetiver, clover, and bare soil. They found that vetiver had the most significant reinforcing effect on the slope. Yang et al. [20] quantified the impact of herbaceous plant root systems on slope stability from the perspective of safety factors, and found that there is an optimal angle at which root systems contribute to improved slope stability.

Totally speaking, previous studies have rarely considered the influence of vegetation root reinforcement on slope stability of expansive soil under rainfall and moisture-induced swelling conditions. Then, this study focuses on investigating the effect of vegetation root reinforcement on the stability of expansive soil slopes under the conditions of moisture absorption and swelling.

2. Model Establishment

2.1. The Principle of Fluid–Structure Interaction in ABAQUS

Soil consists of a soil skeleton and voids. Rainfall infiltrating into the voids of the slope soil generates a hydraulic head difference. This difference in hydraulic head induces water flow in the soil, leading to the formation of seepage forces acting on the soil and causing changes in the stress field. The changes in the stress field cause deformation in the soil, resulting in alterations in the internal void volume of the soil, subsequently leading to changes in the soil permeability coefficient, ultimately affecting the soil's seepage field. ABAQUS analyzes the aforementioned fluid–structure interaction problem based on the principles of mass conservation and the virtual work principle. It adopts a coupling algorithm based on the Biot consolidation theory to compute the equilibrium equation of stress seepage and the transient seepage equation. By combining pore pressure boundaries with flow rate boundary conditions, the finite element equations for the permeability–stress coupling are obtained and subsequently solved.

2.2. Considering the Shear Strength of Reinforced Unsaturated Soil with Root Reinforcement

Unsaturated soil needs to consider the soil softening caused by pore water, so its shear strength is often determined using the Fredlund unsaturated strength theory [21]. Considering root reinforcement, JWI [22] and Wu [23] have made corresponding modifications, which are expressed as follows:

$$\tau_f = c' + (\sigma_n - u_a)\tan\varphi' + (u_a - u_w)\tan\varphi^b + \Delta S \tag{1}$$

$$\Delta S = \frac{A_r T}{A}(\sin\beta + \cos\beta\tan\varphi) \tag{2}$$

$$T = (4\tau^f EZ/D)^{\frac{1}{2}} \tag{3}$$

Here, τ_f represents the shear strength of the soil; c' represents the effective cohesion of the soil; σ_n represents the total stress generated by the self-weight and external loads on the soil; φ' represents the effective friction angle of the soil; u_a represents the pore air pressure; u_w represents the pore water pressure; φ^b represents the angle that changes due to variations in pore water pressure; T represents the maximum tensile stress in the roots; A_r/A represents the ratio of the cross-sectional area of the roots to the area of the soil section; τ^f represents the tangential frictional force between the roots and the soil; E represents the elastic modulus of the roots; Z represents the width of the shearing zone; D represents the diameter of the roots; and β represents the angle between the roots and the shearing plane. Since the slope surface is connected to the atmosphere, the pore air pressure can be considered as 0, and negative pore water pressure can represent matric suction.

During computation, ABAQUS obtains the saturation of each node, and then, based on the soil–water characteristic curve, it determines the corresponding matric suction for the node. This value is then substituted into Equations (1)–(3) to calculate the shear strength of the node.

2.3. Simulation of Volume Changes in Expansive Soils

The expansion principle of expansive soil is similar to the thermal expansion and contraction of materials, and the simulation of the moisture field can be based on the temperature field.

Assuming that the swelling of expansive soil upon water absorption is isotropic, the volumetric change does not generate shear stress or shear strain. The total strain component resulting from changes in soil moisture content can be expressed as follows:

$$d\varepsilon_{ij} = d\varepsilon_{ij}^w = \alpha\delta_{ij}dw \tag{4}$$

Here, $d\varepsilon_{ij}^w$ represents the incremental strain due to changes in moisture content; α represents the isotropic moisture expansion coefficient; δ_{ij} represents the Kronecker delta symbol; and dw represents the incremental change in moisture content.

The total strain increment caused by thermal expansion of the material is expressed as:

$$d\eta_{ij} = d\eta_{ij}^h = \beta\delta_{ij}dT \tag{5}$$

Here, $d\eta_{ij}^h$ is the strain increment due to temperature; β is the isotropic thermal expansion coefficient; δ_{ij} is Kronecker delta symbol; and dT is the temperature increment.

Magnitude relationship between temperature and moisture content:

$$\alpha = 100\beta \tag{6}$$

Volume changes in expansive soils with changes in soil moisture content are implemented by programming ABAQUS subroutines USDFLD and UEXPAN. The subroutine GETVRM is used to obtain the saturation of each node, and through the transformation of

Equations (4)–(6), the volumetric strain variations with changes in the moisture field are ultimately obtained.

2.4. Strength Reduction Method

The stability of slopes is generally evaluated by the safety factor, and the strength reduction method is one of the commonly used methods to calculate the safety factor of slopes. In this method, the stress state of the soil remains unchanged, and the shear strength of the slope is reduced by a reduction factor (*Fr*). The reduction parameter for the shear strength of the soil, based on the Mohr–Coulomb yield criterion, is as follows:

$$c' = c/Fr \tag{7}$$

$$\varphi' = \arctan(\tan\varphi/Fr) \tag{8}$$

Using ABAQUS, strength reduction is implemented by applying field variables. The controlled soil shear strength parameters are successively reduced. When the soil undergoes plastic strain localization due to strength reduction or when there is a sudden large displacement at monitoring points, it is considered as slope instability. The corresponding reduction coefficient value represents the safety factor of the slope.

2.5. Geometric Model and Material Parameters

2.5.1. Geometric Model of the Slope

The geometric model of the slope is shown in Figure 1. The soil is considered as an ideal elastoplastic material, which following the Mohr–Coulomb strength criterion. An 8-node three-dimensional strain pore pressure element (C3D8P) is used to discretize the model. The expansive soil slope has a height of 14 m at the crest and 6 m at the toe, with a slope ratio of 2:3. The width of the slope at the crest and toe is 5 m. The slope soil is divided into three layers: the upper layer is the weathered expansive soil layer with a thickness of 1.5 m, the middle layer is the un-weathered expansive soil layer with a thickness of 1.5 m at the toe and 9.5 m at the crest, and the lower layer is the stiff clay layer with a thickness of 3 m. The total thickness of the three-dimensional slope model is taken as 7 m. The temperature equivalent coefficient of soil expansion is taken as 1×10^{-4} based on reference [4]. The material parameters are provided in Table 1. The slope layer A is the weathered soil layer with developed cracks, and its permeability coefficient is 1000 times that of layer B (un-weathered layer) [24].

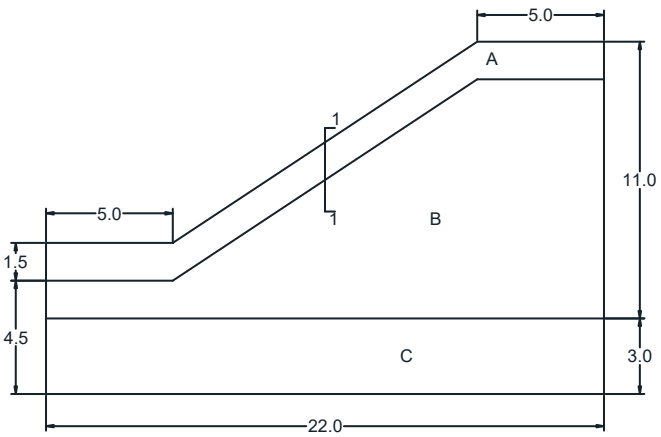


Figure 1. Geometric model of the slope (unit: m).

Table 1. Material parameters of soil layers.

Soil Layer Number	Elastic Modulus (MPa)	Poisson's Ratio	Unit Weight (kg/m^3)	Cohesion (KPa)	Friction Angle (°)	Permeability Coefficient (cm/s)
A	15	0.35	1900	15	11	2.0×10^{-3}
B	15	0.35	1900	38.7	18	1.2×10^{-6}
C	25	0.32	2000	700	36	8.5×10^{-7}

The mesh division is shown in Figure 2. The mesh control employs sweep hexahedral elements, with a grid size of 0.25 m × 0.25 m × 0.25 m for the shallow layer (A). To ensure a smooth transition in the mesh division, the left part of the bottom layer (C) is consistent with the grid size of the shallow layer (A). The grid size on the right side of the bottom layer (C) is 0.5 m × 0.5 m × 0.5 m, with a natural transition set for the right side of the middle layer (B).

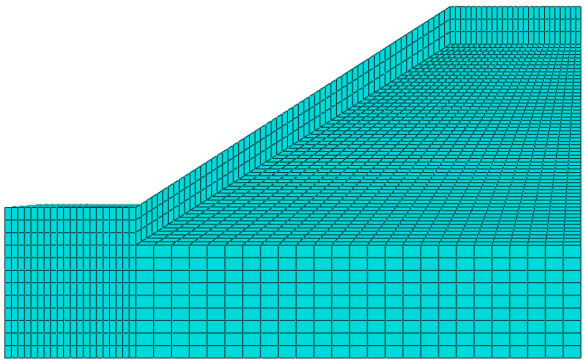


Figure 2. Mesh division for the slope model.

2.5.2. Hydraulic Characteristic Parameters of the Soil

The permeability coefficient of unsaturated soil is related to matric suction and volumetric water content. And the soil permeability coefficient varies with changes in matric suction [25]:

$$K_w = a_w K_{ws} / [a_w + (b_w \times (u_a - u_w))^{c_w}] \quad (9)$$

Here, K_{ws} is the permeability coefficient of soil when saturated; u_a is the pore air pressure (assumed to be 0); u_w is the pore water pressure; and a_w, b_w, and c_w are material coefficients with values of 1000, 0.01, and 1.7, respectively, as given in reference [16].

The relationship between saturation degree and matric suction variation is as following [25]:

$$S_r = S_i + (S_n - S_i) a_s / [a_s + (b_s \times (u_a - u_w))^{c_s}] \quad (10)$$

Here, S_r is the saturation degree; S_i is the residual saturation degree (taken as 0.08); S_n is the maximum saturation degree (taken as 1); and a_s, b_s, and c_s are material coefficients, with values of 1, 5×10^{-5}, and 3.5, respectively, as reported in reference [16].

2.5.3. Poinsettia Root System Model

Poinsettia belongs to the category of species with a diffuse root system. The dominance of the taproot is not significant, and the lateral roots are well developed, with an average diameter of 1.94 mm and relatively long length [26]. The root system of a single poinsettia plant consists of one main root and twelve lateral roots, with a diameter of 2.0 mm, an elastic modulus of 789.62 MPa [27], and a Poisson's ratio of 0.25 [28]. The angle between the main root and the lateral roots is set at 60° [12]. The length of the main root is 2000 mm, and the length of the lateral roots is 500 mm.

The root system of the poinsettia plant is modeled using an ideal elastic model, considered as a truss structure. The simulation is conducted using three-dimensional beam

elements, specifically the T3D2 elements. To avoid any intersections between roots during the simulation, the spacing between poinsettia plants is increased. A plant spacing of 1 m and row spacing of 1 m are set for this purpose.

2.6. Boundary Conditions and Constraints

The initial void ratio of the expansive soil is supposed to be 1.0. The initial groundwater level is located at the surface of the slope foot and the water pressure is set to be $10 \times (6 - Y)$ kPa, where Y is the height of the slope foot. The bottom and two sides of the model are considered impermeable boundaries by default. The lateral displacements in the x and z directions of the slope model are constrained, allowing only displacements in the y direction. The bottom surface is fully fixed, preventing any movement.

For the model calculation, a root–soil separation approach is adopted, where different material parameters are assigned to the soil and root system. The contact interface between the root system and soil is implemented using the Abaqus embedded region feature within the constraints. This ensures that the nodes have the displacement degrees of freedom corresponding to the respective positions of the solid elements (soil).

2.7. Rainfall Load

Rainfall is simulated by applying flow boundary on the surface of the slope. And rainfall boundary conditions are set to the top surface and slope surface of the slope. The duration and amplitude of the rainfall are shown in Figure 3, with a total duration of 120 h. The rainfall conditions are summarized in Table 2.

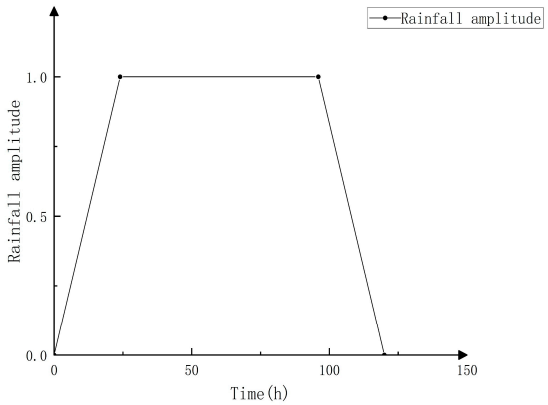


Figure 3. Rainfall process.

Table 2. Rainfall scheme.

Operating Condition Number	Rainfall Intensity (mm/d)	Time (h)	Rainfall Grade
Operating condition 1	10	120	Moderate rain
Operating condition 2	30	120	Heavy rain
Operating condition 3	60	120	Torrential rain
Operating condition 4	120	120	Heavy rainstorm

3. Results Analysis

3.1. The Influence of Rainfall on the Moisture Field of the Slope

Figure 4 shows the saturation degree distribution map of the slope after rainfall. Due to the significantly higher permeability coefficient of the weathered layer compared to the non-weathered layer, the wetting front gradually advances from the weathered layer to the non-weathered layer during the rainfall process, exhibiting a distinct sharp angle. The saturated zone also continuously moves up from the slope toe, and the saturation rate

of the weathered layer is higher than that of the non-weathered layer. These results are consistent with the infiltration pattern of unsaturated rainfall.

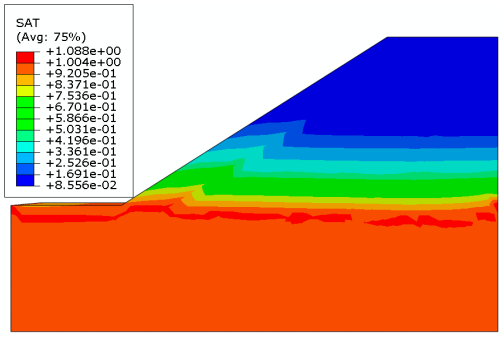


Figure 4. Image depicting the saturation distribution of the slope after the rainfall has ended (condition 4).

3.2. Effect of Expansion on Slope Displacement

The final displacement contour maps considering swelling under various rainfall conditions are shown in Figure 5. Table 3 presents the maximum displacement values considering swelling and no swelling for each rainfall condition. The maximum displacements considering swelling are one order of magnitude larger than those without considering swelling, for the same rainfall condition.

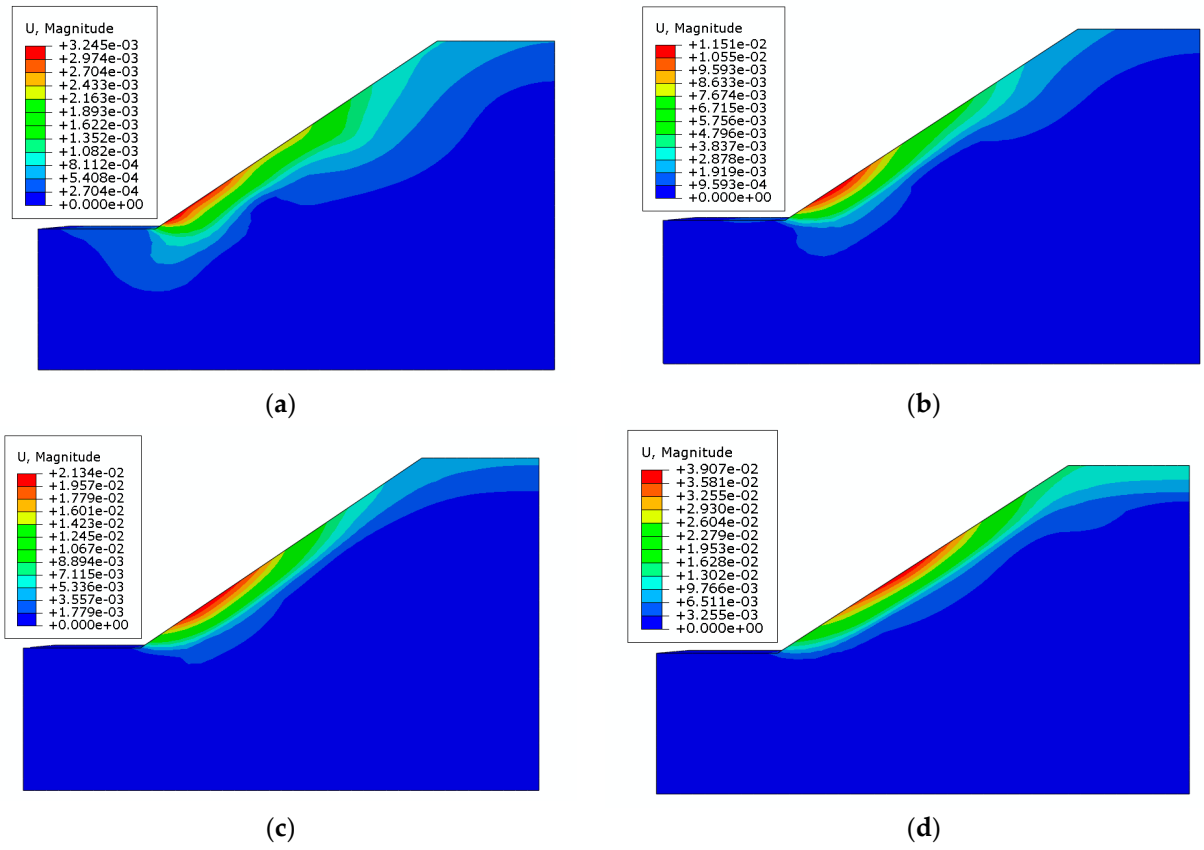


Figure 5. Contour map of displacement considering expansion effect (unit: m): (**a**) Condition 1, (**b**) Condition 2, (**c**) Condition 3, (**d**) Condition 4.

Table 3. Maximum displacement calculation results with and without considering expansion.

Rainfall Conditions			Without Considering Expansion	Consider Expansion
Rainfall Conditions	**Rainfall Intensity (mm/d)**	**Rainfall Duration (h)**	**Maximum Displacement (m)**	**Maximum Displacement (m)**
Condition 1	10	120	1.947×10^{-4}	3.245×10^{-3}
Condition 2	30	120	5.670×10^{-4}	1.151×10^{-2}
Condition 3	60	120	1.223×10^{-3}	2.134×10^{-2}
Condition 4	120	120	4.169×10^{-3}	3.907×10^{-2}

Considering the factor of swelling deformation, the potential sliding surface of the slope may traverse the entire slope surface, located at the interface between the weathered layer and the un-weathered layer, and tangent to the interface. The maximum displacement of the slope gradually increases with rainfall intensity increase. Shallow layer sliding first occurs at the toe of the slope, and with the increase in rainfall duration, the sliding area gradually expands upward along the slope. The depth of the sliding surface deepens with an increase in rainfall duration, ultimately stopping at the interface between the weathered layer and the un-weathered layer. Considering that the slope failure of expansive soil mainly occurs in the shallow layer and exhibits a cohesive nature, the upward expansion of the sliding area is due to the sliding of the soil at the toe of the slope, which reduces the support to the upper part soil and consequently decreases tits shear strength, leading to its movement. Therefore, the influence of moisture-induced swelling cannot be ignored when calculating slope stability.

3.3. Effect of Reinforced Oleander Root System on Slope Displacement

The displacement contour maps considering vegetation root reinforcement for each rainfall condition are shown in Figure 6. The maximum displacements are presented in Table 4. It can be observed from Table 4 that regardless of whether vegetation root reinforcement is considered or not, the maximum slope displacement increases with increasing rainfall intensity. Rainfall intensity is one of the important factors to be considered in slope safety design.

The surface layer of the slope is weathered and prone to hygroscopic expansion and desiccation cracking, resulting in numerous cracks on the surface. The permeability coefficient of the surface layer is relatively high. Rainwater erosion can easily lead to shallow instability of expansive soil slopes [29]. The saturation degree of the surface layer increases gradually with the increasing rainfall intensity, leading to a decrease in effective shear strength in the surface layer. As a result, the maximum slope displacement gradually increases. The root systems of vegetation form a chain reaction with soil particles [30], which enhances the shear resistance of the surface soil, restraining the upward movement of the zone where shear strength decreases.

From a stress perspective, the maximum stress in a vegetation-reinforced slope is concentrated at the nodes where the vegetation roots are located. The vegetation roots enhance the shear strength of the soil by approximately three orders of magnitude, as shown in Table 5. The roots restrict the displacement of the surface soil layer, which is equivalent to increasing the cohesion of that layer and improved soil erosion resistance [31]. This forms a network reinforcement within the soil, improving the overall stiffness of the soil layer and reducing the displacement of the surface layer of the slope.

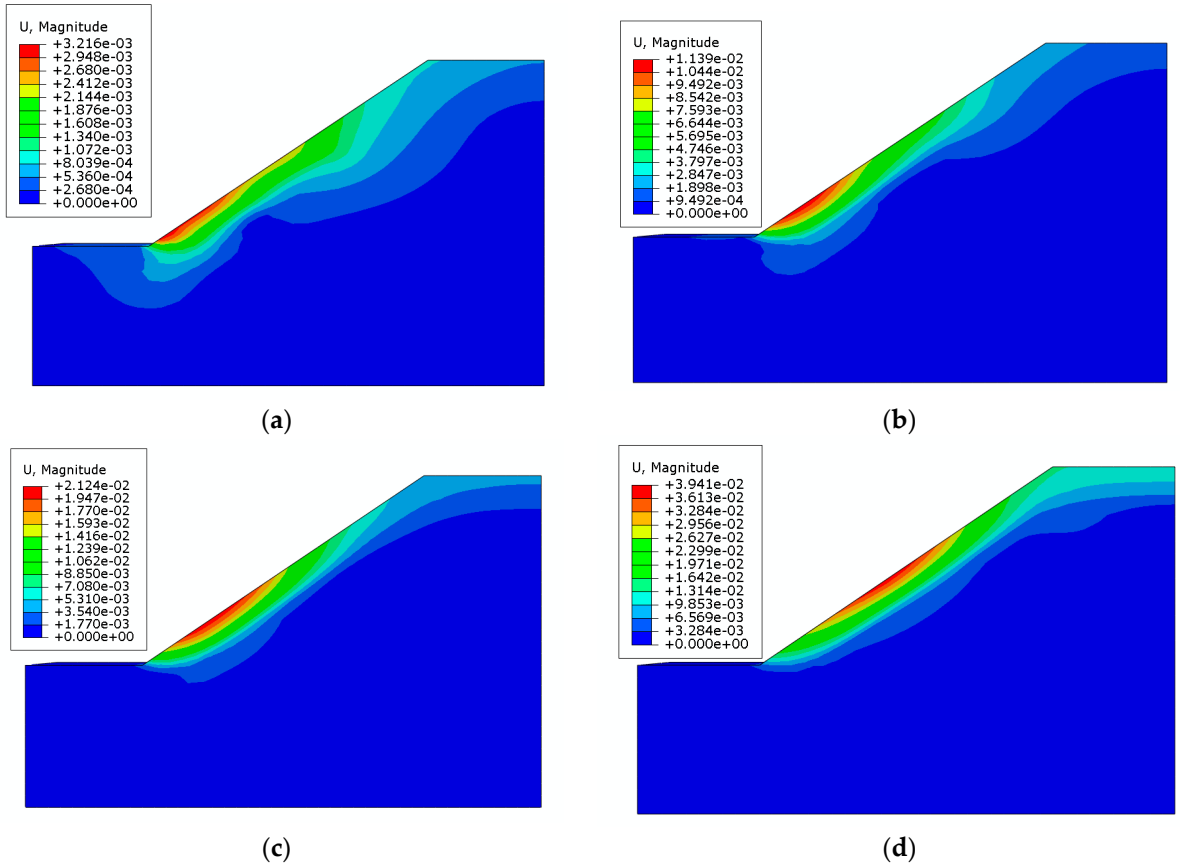


Figure 6. Displacement calculation contour plot with reinforcement considered (unit: m): (**a**) Condition 1, (**b**) Condition 2, (**c**) Condition 3, (**d**) Condition 4.

Table 4. Maximum displacement with/without reinforcement considered.

Rainfall Conditions			Without Considering Expansion	Consider Expansion
Rainfall Conditions	**Rainfall Intensity (mm/d)**	**Rainfall Duration (h)**	**Maximum Displacement (m)**	**Maximum Displacement (m)**
Condition 1	10	120	3.245×10^{-3}	3.216×10^{-3}
Condition 2	30	120	1.151×10^{-2}	1.139×10^{-2}
Condition 3	60	120	2.134×10^{-2}	2.124×10^{-2}
Condition 4	120	120	3.907×10^{-2}	3.941×10^{-2}

Table 5. Maximum horizontal stress with/without reinforcement considered.

Rainfall Conditions			Without Considering Expansion	Consider Expansion
Rainfall Conditions	**Rainfall Intensity (mm/d)**	**Rainfall Duration (h)**	**Maximum Horizontal Stress (Pa)**	**Maximum Horizontal Stress (Pa)**
Condition 1	10	120	-2.569×10^{3}	1.913×10^{6}
Condition 2	30	120	4.829×10^{4}	5.896×10^{6}
Condition 3	60	120	5.998×10^{4}	1.093×10^{7}
Condition 4	120	120	8.846×10^{4}	1.932×10^{7}

Under the same rainfall conditions, the maximum displacement of the reinforced expansive soil slope will decrease. However, when the rainfall intensity exceeds the permeability coefficient of the slope (in the case of Condition 4), the maximum displacement of the slope actually increases. This is because the rainfall intensity exceeds the infiltration capacity of the slope, and the excess water forms surface runoff, causing erosion of the surface soil layer. The shallow water content of the slope increases rapidly with rainfall time. When the soil moisture content reaches a relatively large value, the effect of the root system on the increase in soil cohesion is not significant [32]. The soil in the weathered zone gradually heals with increasing saturation, and the sliding tendency shifts from deeper layers to shallower layers. In the shallow soil layer, only the main roots exist, and they do not form a reinforced network with the secondary roots. As a result, the overall stiffness enhancement is not significant.

3.4. Influence of Reinforcement on Horizontal Stress in Slope

Figure 7 shows the horizontal stress profiles within a depth range of 5 m in the slope, as indicated by the location "1-1" in Figure 1. The horizontal stress profiles within this depth range exhibit an inverted "V" shape, with the magnitude of increase becoming larger as the rainfall intensity increases. A sharp change in horizontal stress occurs within the depth range of 1–2 m. The impact of reinforcement on horizontal stress differs in the surface layer. For rainfall conditions of Case 1 and Case 2, where the rainfall intensity is low, the horizontal stress profiles are nearly overlapped regardless of reinforcement. However, for Case 3 and Case 4, where the rainfall intensity is relatively high, the horizontal stress profiles show separation. At a depth of 0 m for Case 3, the reinforced horizontal stress is reduced by 26.3%. At a depth of 0.9 m, the reinforced horizontal stress increases by 2.9%. At a depth of 1.9 m, the reinforced horizontal stress decreases by 1.4%. For Case 4, at a depth of 0 m, the reinforced horizontal stress increases by 12.0%. At a depth of 0.9 m, the reinforced horizontal stress increases by 16.68%. At a depth of 1.9 m, the reinforced horizontal stress decreases by 0.3%.

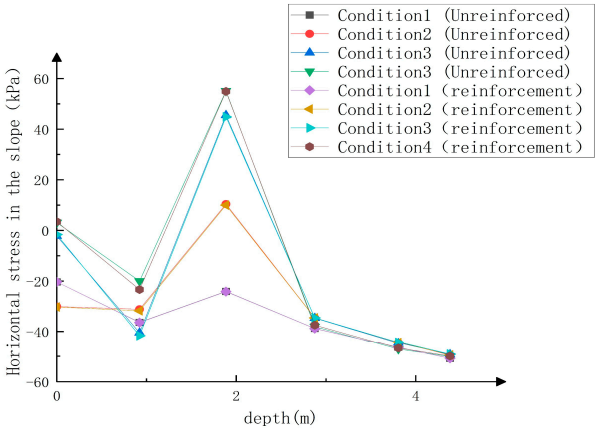


Figure 7. Horizontal stress in the slope.

The top of the "V" shape corresponds to the shallow layer (weathered layer) and the interface between the intermediate layer (non-weathered layer). The sliding tendency in the shallow layer increases with increasing rainfall intensity. As the rainfall ends, the expansion deformation of the slope's weathered layer reaches its maximum, leading to a significant difference in expansion deformation between the weathered layer and the non-weathered layer. This results in a large sharp change in horizontal stress at the interface between the two layers. Compared to the stress generated by the differential expansion deformation, the resistance provided by vegetation reinforcement is limited. Therefore, when the rainfall intensity is low, the horizontal stress profiles with and without reinforcement tend to overlap. However, as the rainfall intensity increases to Case 3 and

Case 4, the sliding tendency in the shallow layer becomes more significant, and some of the stress is transmitted to the non-weathered layer through the root system. Thus, the effect of reinforcement is more pronounced in Case 3 and Case 4 compared to Case 1 and Case 2. Vegetation reinforcement can alter the stress field in the slope, but the changes are limited.

3.5. The Influence of Reinforcement on the Plastic Zone of the Slope

This study primarily focuses on the analysis of shallow slope layer stability, specifically considering the reduction in strength parameters for the surface layer (weathered layer) soil. The final plastic zone diagrams are calculated for both reinforced and unreinforced conditions under various scenarios.

The final plastic zone diagrams for different scenarios under the unreinforced condition are similar. Taking Scenario 4 as an example (represented in Figure 8), it can be observed that the plastic zone is fully connected without reinforcement, and the area with the highest plastic strain values is concentrated at the interface between the weathered layer and the un-weathered layer. The shape of the plastic zone is characterized by regular rectangular strips, with a tendency to extend towards deeper layers.

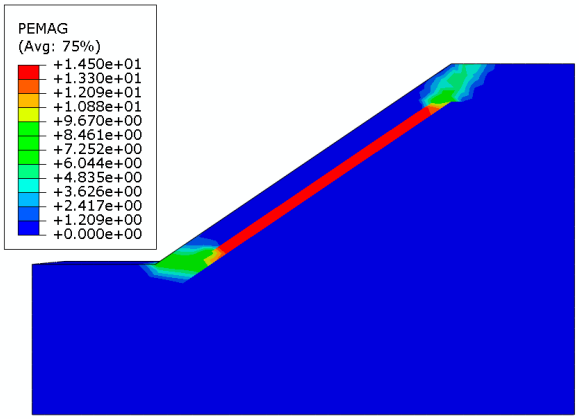


Figure 8. Final plastic zone diagram without reinforcement (Condition 4).

Figure 9 shows the final plastic zone diagrams for the four scenarios after reinforcement. Similarly to the unreinforced condition, the plastic zone is fully connected, and the maximum plastic strain values occur at the interface between the weathered layer and the un-weathered layer. However, there is no presence of a concentrated area with a regular strip-like pattern. The soil's plastic strain around the roots exhibits a uniform undulating pattern along the slope, with the peaks corresponding to the locations of the main plant roots. As the rainfall intensity increases, the angles of the undulations become smaller, and the region with the maximum plastic strain values shifts from the slope's top to the bottom.

In this study, the shallow weathered layer is relatively thin, and a portion of the vegetation roots penetrate into the underlying less-weathered layer, allowing the transfer of downward forces from the surface layer to the more stable intermediate layer, thereby delaying the sliding of the surface layer. With the reduction in shear strength and an increase in rainfall intensity, the inherent shear strength of the slope decreases, and the plastic failure zone gradually shifts from the slope toe to the slope crest. The tensile strength of the roots inhibits the development of plastic strain, resulting in a sharp change in the plastic strain region, dispersing the originally concentrated plastic strain along the interface between the two soil layers. However, as the rainfall intensity increases, the dispersing effect gradually weakens, and the sliding tendency of the surface layer increases. As a result, the maximum plastic strain at the point of failure decreases gradually.

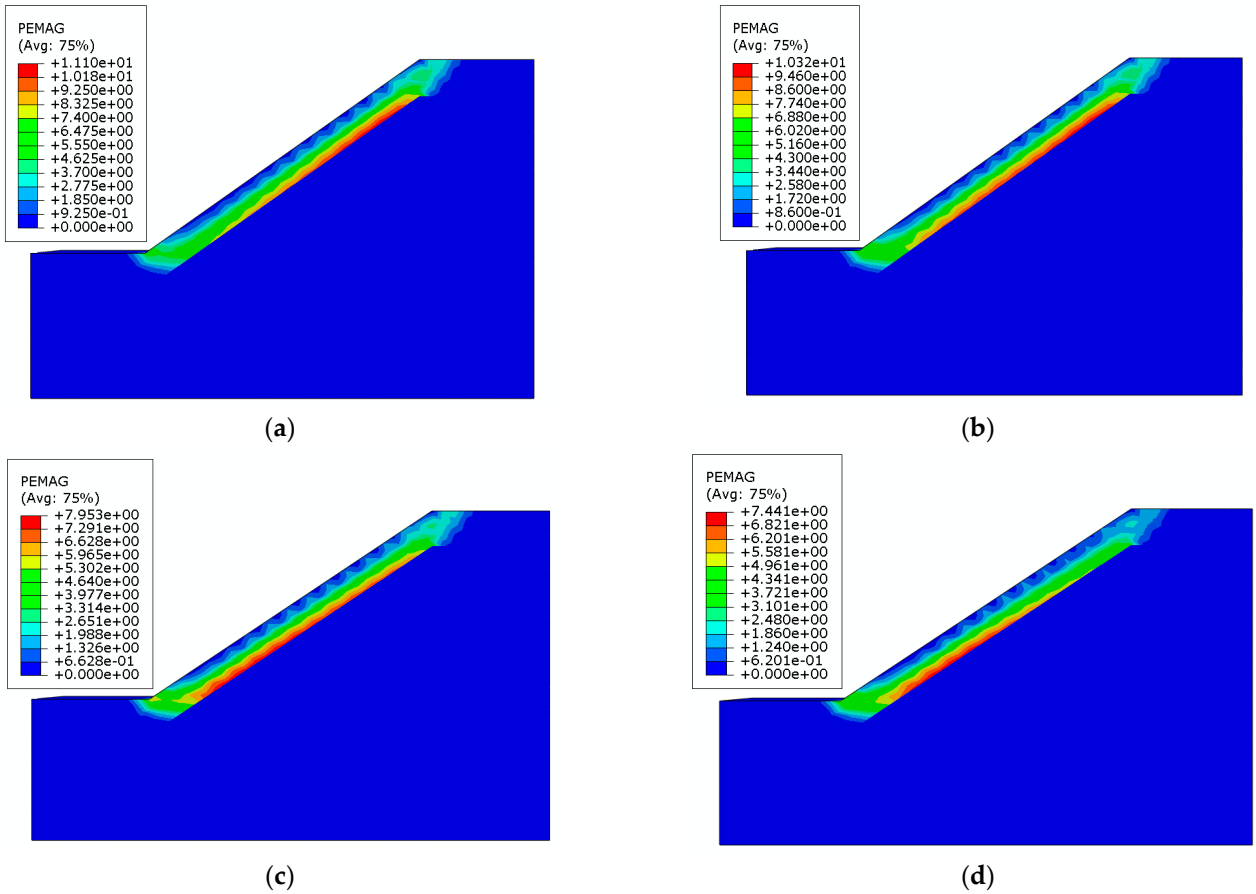


Figure 9. Reinforced plastic zone contour map: (**a**) Condition 1, (**b**) Condition 2, (**c**) Condition 3, (**d**) Condition 4.

The time required for the plastic zone to propagate with and without reinforcement is shown in Table 6, with the default analysis step length set to 1. From Table 6, it can be observed that the reinforced plastic zone requires a longer time step to propagate compared to the unreinforced plastic zone. This indicates that vegetation reinforcement has a positive effect on the stability of the shallow slope. However, in Figure 8, it can be seen that for Condition 4 compared to Condition 3, there is a significant decrease in the maximum plastic strain during the propagation of the plastic zone. In contrast, Table 6 shows that the time step for the plastic zone to propagate in Condition 4, with and without reinforcement, is significantly longer compared to Condition 3. The reason for this discrepancy is that in Condition 3, the development of plastic strain is influenced by the rainfall intensity, while in Condition 4, it depends on the infiltration capacity of the slope. The impact of rainfall infiltration on slope strength is relatively small in Condition 4 compared to Condition 3. Therefore, the reduction in the maximum plastic strain during the propagation of the plastic zone is not significant in Condition 4. However, the transfer of downward forces by the vegetation roots in the surface layer of the slope is not reduced, and it increases with the increase in rainfall intensity. As a result, compared to the unreinforced condition, the duration of plastic zone propagation is significantly longer in Condition 4, resulting in a greater increase in the time required for the plastic zone to propagate.

Table 6. Time steps required for plastic zone propagation with and without reinforcement.

Rainfall Conditions	Time Step Length for Failure without Reinforcement	Time Step Length for Failure with Reinforcement	Percentage Increase
Condition 1	0.6386	0.7965	24.72%
Condition 2	0.6080	0.7628	25.46%
Condition 3	0.5730	0.7212	25.86%
Condition 4	0.4897	0.6318	29.02%

3.6. Effect of Vegetation Root Reinforcement on Slope Stability

In order to visually evaluate the influence of poinsettia root systems on the stability of expansive soil slopes, an analysis was conducted on the displacement variations at the slope crest and toe under four rainfall conditions. The horizontal displacement changes are shown in Figure 10. The presence of roots can delay the development of horizontal displacement on the slope surface, and the trend of the results is consistent with the results of existing studies [33].

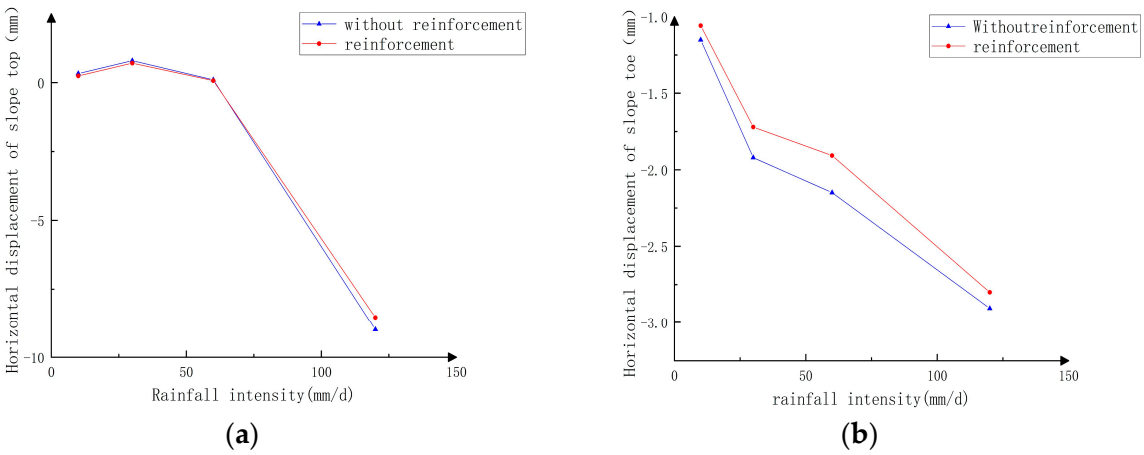


Figure 10. Horizontal displacement change: (**a**) horizontal displacement of slope top; (**b**) horizontal displacement of slope toe.

The model is established in ABAQUS, with the slope direction along the negative *x*-axis. From Figure 10a, it can be observed that with and without reinforcement, the final horizontal displacements at the slope crest for Condition 1 are in the opposite direction to the sliding surface, while for Condition 2, the displacements are also in the opposite direction but larger than those for Condition 1. The sliding pattern appears to be arc-shaped, as shown in Figure 11. The reason for this phenomenon is that after the expansive soil absorbs moisture and expands, its strength decreases, resulting in the formation of a high-stress zone in the surface layer (weathered layer). Under the self-weight accumulation of the slope, sliding occurs first at the slope toe. The vegetation root system increases the stiffness of the surface layer, and the sliding at the slope toe causes rigid body rotation of the surface layer, resulting in displacement of the slope crest along the positive *x*-axis. From the variations in horizontal displacement at the slope crest and toe, it can be observed that considering root reinforcement can limit the horizontal sliding displacement of the slope.

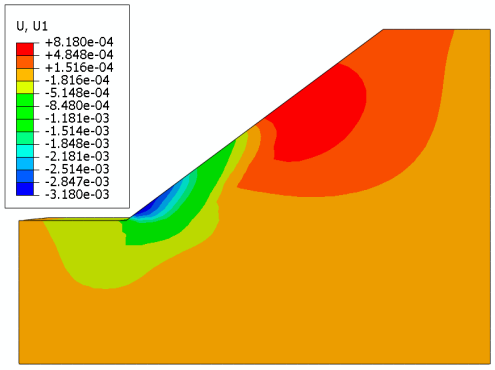


Figure 11. Horizontal displacement cloud map of condition 2 (reinforced) (unit: m).

The slope safety factors were obtained using the strength reduction method, as presented in Table 7. The calculation results indicate that for the expansive soil slope, regardless of whether vegetation reinforcement is considered, the safety factor decreases as the rainfall intensity increases. The larger the increase in rainfall intensity, the greater the decrease in the safety factor and the faster the deterioration in the slope stability. By comparing the safety factors with and without vegetation reinforcement at the same rainfall intensity, the following observations can be made: at a rainfall intensity of 10 mm/d, the safety factor increases by 63.2%; at a rainfall intensity of 30 mm/d, the safety factor increases by 67.7%; at a rainfall intensity of 60 mm/d, the safety factor increases by 73.9%; at a rainfall intensity of 120 mm/d, the safety factor increases by 67.6%. Based on the changes in the safety factor, it can be concluded that vegetation root reinforcement can improve the stability of the surface layer (weathered layer) of the expansive soil slope, and the improvement becomes more significant as the rainfall intensity increases. However, when the rainfall intensity exceeds the infiltration capacity of the slope, the ability of the safety factor to increase starts to decline. Plant root systems have strong tensile and shear strength, and they play a significant role when the slope gradually becomes unstable under high rainfall intensity. The reason for the decrease is that the rainfall intensity exceeds the infiltration capacity of the slope, causing the moisture content and the resulting expansion stress of the surface soil to reach their peaks. This will reduce the shear strength provided by the root reinforcement, leading to a decrease in the effectiveness of reinforcement.

Table 7. Safety factor (reinforced and unreinforced).

Rainfall Conditions			Unreinforced	Reinforced
Rainfall Conditions	**Rainfall Intensity (mm/d)**	**Rainfall Duration (h)**	**Safety Factor (Fs)**	**Safety Factor (Fs)**
Condition 1	10	120	2.04	3.33
Condition 2	30	120	1.98	3.32
Condition 3	60	120	1.88	3.27
Condition 4	120	120	1.70	2.85

4. Conclusions

The main conclusions of this study regarding the impact of poinsettia root reinforcement on the stability of expansive soil slopes, considering the effects of moisture absorption and expansion, can be summarized from four perspectives: displacement variation, plastic zone variation, horizontal stress variation, and safety factor variation:

(1) Poinsettia root reinforcement can reduce the displacement variation. When the rain fall intensity is 10 mm/d, the displacement is reduced by 0.89%; when the rainfall intensity is 30 mm/d, the displacement is reduced by 1.04%; when the rainfall intensity is 60 mm/d, the displacement is reduced by 0.47%; and when the rainfall intensity is

120 mm/d, the displacement increases by 0.87%. However, the consolidation effect decreases when the rainfall intensity exceeds the soil permeability coefficient.

(2) The final plastic zone diagram of the expansive soil slope is calculated using the strength reduction method. Without reinforcement, the plastic zone appears as a regular strip-shaped area concentrated at the interface between the weathered layer and the un-weathered layer. Poinsettia root reinforcement can alleviate the concentration of plastic strain, disperse the plastic zone, and distribute along the shape of the roots, thus increasing slope stability.

(3) Poinsettia root reinforcement can increase the safety factor of the shallow slope. When the rainfall intensity is 10 mm/d, the safety factor increases by 63.2%; when the rainfall intensity is 30 mm/d, the safety factor increases by 67.7%; when the rainfall intensity is 60 mm/d, the safety factor increases by 73.9%; and when the rainfall intensity is 120 mm/d, the safety factor increases by 67.6%. The increase in safety factor becomes greater as the rainfall intensity increases. However, when the rainfall intensity exceeds the surface permeability coefficient, the enhancement effect of reinforcement decreases.

Author Contributions: writing—original draft preparation, software, Y.W.; writing—review and editing, Conceptualization, methodology, W.X.; validation, software, Z.W.; data curation, software, Y.Z. All authors have read and agreed to the published version of the manuscript.

Funding: This research received no external funding.

Institutional Review Board Statement: Not applicable.

Informed Consent Statement: Not applicable.

Data Availability Statement: All the analysis data in this paper are from the numerical simulation carried out with finite element software, which was performed to ensure the truth and validity of the data.

Conflicts of Interest: The authors declare no conflict of interest.

References

1. Liu, T.-H. *The Problem of Expansive Soil in Engineering Construction*; China Architecture & Building Press: Beijing, China, 1997.
2. Wang, A.-J.; Li, X.-W.; Dai, G.-Z. Influence of desorption moisture state on the swelling deformation and shear strength characteristics of expansive soil. *Geotech. Investig. Surv.* **2012**, *40*, 1–4+26.
3. Xiao, J.; Tan, Y.-F.; Tong, C.; Yang, H.-P.; Chang, J.; Zhou, W.-L.; Chen, G.-Y. Numerical Analysis for Shallow Landslides of Expansive Soil Slopes Based on Three Fields Coupling. *Ind. Constr.* **2022**, *52*, 128–136+118. [CrossRef]
4. Zhao, S.-Y.; Shi, Z.-M.; Bao, Y.-N.; Zhou, H.-R.; Peng, M. Stability analysis of expansive soil slope considering seepage softening and moistening swelling deformation. *J. Eng. Geol.* **2021**, *29*, 777–785. [CrossRef]
5. Zhang, B.; Fan, Q.; Luo, J.; Mei, G. A New Analysis Method Based on the Coupling Effect of Saturation and Expansion for the Shallow Stability of Expansive Soil Slopes. *Symmetry* **2022**, *14*, 898. [CrossRef]
6. Xiao, J.; Yang, H.-P.; Zhang, J.-H.; Tang, X.-Y. Surficial Failure of Expansive Soil Cutting Slope and Its Flexible Support Treatment Technology. *Adv. Civ. Eng.* **2018**, *2018*, 1609608. [CrossRef]
7. He, P.; Li, S.-C.; Xiao, J.; Zhang, Q.-Q.; Xu, F.; Zhang, J. Shallow Sliding Failure Prediction Model of Expansive Soil Slope based on Gaussian Process Theory and Its Engineering Application. *KSCE J. Civ. Eng.* **2018**, *22*, 1709–1719. [CrossRef]
8. Ng, C.W.W.; Kamchoom, V.; Leung, A.K. Centrifuge modelling of the effects of root geometry on transpiration-induced suction and stability of vegetated slopes. *Landslides* **2016**, *13*, 925–938. [CrossRef]
9. Wu, M.-S.; Zhou, C.; Wang, L.; Tan, C.-M. Numerical simulation of the influence of roots and fissures on hydraulic and mechanical characteristics of the soil. *Rock Soil Mech.* **2019**, *40* (Suppl. S1), 519–526+534. [CrossRef]
10. Wu, H.-W. Atmosphere-plant-soil interactions: Theories and mechanisms. *Chin. J. Geotech. Eng.* **2017**, *39*, 1–47.
11. Thomas, R.E.; Pollen-Bankhead, N. Modeling root-reinforcement with a fiber-bundle model and Monte Carlo simulation. *Ecol. Eng.* **2010**, *36*, 47–61. [CrossRef]
12. Reubens, B.; Poesen, J.; Danjon, F.; Geudens, G.; Muys, B. The role of fine and coarse roots in shallow slope stability and soil erosion control with a focus on root system architecture: A review. *Trees Struct. Funct.* **2007**, *21*, 385–402. [CrossRef]
13. Fan, C.-C.; Tsai, M.-H. Spatial distribution of plant root forces in root-permeated soils subject to shear. *Soil Tillage Res.* **2016**, *156*, 1–15. [CrossRef]

14. Ji, X.-L.; Yang, P. The effect of bermuda grass root morphology on the displacement of slope. In Proceedings of the 1st International Conference on Advances in Civil Engineering and Materials and 1st World Symposium on Sustainable Bio-Composite Materials and Structures, ACEM 2018 and SBMS 2018, Nanjing, China, 9–11 November 2018; EDP Sciences: Nanjing, China, 2019.
15. Preti, F.; Dani, A.; Laio, F. Root profile assessment by means of hydrological, pedological and above-ground vegetation information for bio-engineering purposes. *Ecol. Eng.* **2010**, *36*, 305–316. [CrossRef]
16. Kokutse, N.K.; Tranquille Temgoua, A.G.; Kavazovic, Z. Slope stability and vegetation: Conceptual and numerical investigation of mechanical effects. *Ecol. Eng.* **2016**, *86*, 146–153. [CrossRef]
17. Capobianco, V.; Robinson, K.; Kalsnes, B.; Ekeheien, C.; Hoydal, O. Hydro-Mechanical Effects of Several Riparian Vegetation Combinations on the Streambank Stability-A Benchmark Case in Southeastern Norway. *Sustainability* **2021**, *13*, 4046. [CrossRef]
18. Sui, Z.; Yuan, W.; Yi, W.; Yang, W. Stability Analysis of Ecological Slopes Based on a 3D Finite Element Model. *Adv. Mater. Sci. Eng.* **2021**, *2021*, 3785943. [CrossRef]
19. Sun, Y.; Gu, X.; Xu, X. Ecological restoration and mechanical reinforcement effect of slope of tailings reservoir. *Environ. Earth Sci.* **2021**, *80*, 1–12. [CrossRef]
20. Yang, Y.; Wang, J.; Duan, Q.; Su, C.; Yan, M.; Dong, Y. The Investigation and 3D Numerical Simulation of Herb Roots in Reinforcing Soil and Stabilizing Slope. *KSCE J. Civ. Eng.* **2018**, *22*, 4909–4921. [CrossRef]
21. Fredlund, D.G.; Rahardjo, H. *Soil Mechanics for Unsaturated Soils*; John Wiley & Sons: New York, NY, USA, 1993; pp. 286–321.
22. Waldron, L.J. The shear resistance of root-permeated homogenous and stratified soil. *Soil Sci. Soc. Am. J.* **1977**, *41*, 843–849. [CrossRef]
23. Wu, T.H.; McKinnell, W.P., III; Swanston, D.N. Strength of tree roots and landslides on Prince of Wales Island, Alaska. *Can. Geotech. J.* **1979**, *16*, 19–33. [CrossRef]
24. Zhang, L.-J. Stability Analysis of Expansive Soil Slope with Rainfall Infiltration. Ph.D. Thesis, China University of Geosciences (Beijing), Beijing, China, 2016.
25. Cho, S.E.; Lee, S.R. Instability of unsaturated soil slopes due to infiltration. *Comput. Geotech.* **2001**, *28*, 185–208. [CrossRef]
26. Ji, X.-L.; Yang, P. Morphological Indexes of Nerium indicum Root System and Its Effects on the Stability of Slope Surface. *J. Northeast For. Univ.* **2013**, *41*, 71–75. [CrossRef]
27. Ji, X.-L.; Yang, P.; Xia, G.-H. Mechanical property experimental study on nerium oleander roots. *Sci. Technol. Eng.* **2018**, *18*, 110–115.
28. Ji, X.-L.; Yang, P. The effects of roots angles of nerium indicum on the stability of slopes. *Ecol. Environ. Sci.* **2012**, *21*, 1966–1970. [CrossRef]
29. Zhou, F.; Zhang, K.; Tang, Y.C. Research on the Ecological Protection Mechanism and Applied of Expansive Soil Slope. In Proceedings of the 3rd International Conference on Civil Engineering and Transportation (ICCET 2013), Kunming, China, 14–15 December 2013; pp. 359–367.
30. Xu, Y.; Su, C.; Zhu, Q.; Yang, C.; Yang, Y. Field study of a new ecological slope protection method applied to expansive soil slope. *Arab. J. Geosci.* **2021**, *14*, 2871. [CrossRef]
31. Wang, G.-Y.; Zhou, H.; Xia, Y.-Q.; Sha, L.-C.; Zhou, H.-G. Experiment on Effect of Grass Root System on Slope Soil Strength and Disintegration Characteristics. *Zhongguo Gonglu Xuebao/China J. Highw. Transp.* **2018**, *31*, 234–241. [CrossRef]
32. Wang, G.Y.; Huang, Y.G.; Li, R.F.; Chang, J.M.; Fu, J.L. Influence of vetiver root on strength of expansive soil-experimental study. *PLoS ONE* **2020**, *15*, e244818. [CrossRef]
33. Yuan, Z.-H.; Deng, Z.-B.; Xie, Q.; Lv, J.; Zhao, H.; Pan, X.-D. Effects of root species and content on soil strength and slope stability. *J. Zhejiang Univ. Technol.* **2022**, *50*, 498–505.

Disclaimer/Publisher's Note: The statements, opinions and data contained in all publications are solely those of the individual author(s) and contributor(s) and not of MDPI and/or the editor(s). MDPI and/or the editor(s) disclaim responsibility for any injury to people or property resulting from any ideas, methods, instructions or products referred to in the content.